E3-2010-144

G. G. Bunatian*, V. G. Nikolenko, A. B. Popov

ON THE E-LINAC-BASED NEUTRON YIELD

Submitted to «Ядерная физика»

*E-mail: bunat@cv.jinr.dubna.ru

Бунатян Г. Г., Николенко В. Г., Попов А. Б. Е3-2010-144
К получению нейтронов на линейных ускорителях электронов

Рассмотрено производство нейтронов в материалах с большим атомным номером в фотоядерных реакциях, вызываемых тормозным излучением потока электронов линейного ускорителя. Исследован выход нейтронов для различных материалов в зависимости от энергии электронов и от размера облучаемого образца. Расчеты выполнены без обращения к «численной симуляции Монте-Карло». Найденные выходы нейтронов соответствуют данным, установленным в исследованиях нейтронных источников, использующих линейные ускорители электронов.

Работа выполнена в Лаборатории нейтронной физики им. И. М. Франка ОИЯИ.

Препринт Объединенного института ядерных исследований. Дубна, 2010

Bunatian G. G., Nikolenko V. G., Popov A. B. E3-2010-144
On the E-Linac-Based Neutron Yield

We treat neutron generating in high atomic number materials due to the photonuclear reactions induced by the bremsstrahlung of an electron beam produced by linear electron accelerator (e-linac). The dependence of neutron yield on the electron energy and the irradiated sample size is considered for various sample materials. The calculations are performed without resort to the so-called «numerical Monte Carlo simulation». The acquired neutron yields are well correlated with the data asserted in investigations performed at a number of the e-linac-driven neutron sources.

The investigation has been performed at the Frank Laboratory of Neutron Physics, JINR.

Preprint of the Joint Institute for Nuclear Research. Dubna, 2010

1. INTRODUCTION. ABOUT PULSED NEUTRON SOURCES

For years, the researches in nuclear fundamental science and technology have steadily been asking for design and construction of neutron sources with various performances and purposes. Among others, the pulsed neutron sources have been serving to explore both neutron interactions with atomic nuclei and structure and dynamics of condensed matter. The primary reactor neutron beams, equipped with mechanical choppers or crystal spectrometers, have been by now superseded by the pulsed spallation neutron sources, cyclotron-based sources (e.g., LAMPF, CERN TOF facility, KFK [1–4]), and by the e-linac-driven neutron sources (e.g., GELINA, ORELA, SACLAY [1, 5–7]) as well. The latter prove now to be quite attractive, notably in the case of high precision cross-section measurements with the time-of-flight method. This is due to their better beam quality and economy aspects, which makes them rather superior to the hadron-driven spallation facilities. This is because the real figure of merit for many experiments is not just the maximum attainable flux, but the flux at a given resolution, which is basically dependent on the arrival time spread of the primary beam and on the artificial pathlengthening of neutron within the radiated target. The contemporary neutron sources driven with the subnanosecond (even a picosecond) pulsing e-linacs provide the best intensity/resolution performance for the neutron TOF spectroscopy between ~ 10 keV and a few MeV neutron energy. These explorations serve to advance in physics and technology of the modern fast fission reactors and the fusion power sources — in a projection into the future. The performances of the e-linac driven sources themselves are actually different, each one is specialized to a quite specified research. In particular, it should well be to point out the very special booster IBR30 [8] that had been used for vast nuclear physics explorations at JINR (Dubna, Russia) for years. Yet a while ago it was put on hold, reaching saturation level of exploitation. A lot of efforts has been devoting in recent years to design and construct at JINR the new facility IREN [9], which was contemplated to replace the IBR30, considered as being its successor. The first stage of this facility operating has by now come online, and it is believed to be competitive in the respective applications with other nowadays available neutron sources.

Though purposes and construction features of various e-linac driven neutron sources are different, the underlying physical processes of neutron production by high energy electrons irradiating large Z targets are actually general. These processes are treated in the work presented in a unified plain way, in the framework of quantum electrodynamics and nuclear physics, making use of reliable experimental data in computations, without having any recourse to the so-called «numerical Monte Carlo simulation». Firstly, in Sec. 2, we describe high energy electron converting in the respective bremsstrahlung, and this bremsstrahlung propagation in a sample, Sec. 3. Generating neutrons by these γ rays are considered in Sec. 4. The total neutron yield in tungsten, uranium, tantalum and lead samples are calculated in Sec. 5 as function of the sample size and the energy and average current of the electron beam irradiating the sample. Surely, many other features of neutron sources are to be considered as their figures of merit: the sample cooling device, the arrangement to operate a sample, the most preferable flight paths and their dispositions, the pulse repetition and the pulse width, etc. These aspects, though extremely important in planning experiments, are outside the scope of the presented study, as asking for a particular treatment for each one given measurement on each given experimental setup.

2. BREMSSTRAHLUNG GENERATING TO YIELD NEUTRONS IN THE PHOTONUCLEAR REACTIONS

As was proclaimed, the purpose is to acquire the neutron production by making use of electron beams delivered by linear electron accelerators, e-linacs. The electron beam, with an electron energy distribution $\rho_e(E_e)$ and a current density $J_e(t)[$ A/cm$^2]$ (generally speaking, time-dependent), travels through the irradiated sample (see Fig. 1) that is prepared of some proper heavy element $A_S(Z_S, N_S)$, such as W, U, Pb, Ta, etc. The bremsstrahlung is thereby induced with the current density

$$J_{S\gamma}(E_\gamma) = \frac{\mathcal{N}_\gamma(E_\gamma)}{\mathrm{s}\cdot\mathrm{cm}^2\cdot\mathrm{MeV}}, \tag{2.1}$$

expressed in terms of the photon number $\mathcal{N}_\gamma(E_\gamma)$ with the energy $E_\gamma = |\mathbf{k}| = k$, per 1 cm^2, 1 s, 1 MeV.

In turn, that γ-ray flux, interacting with nuclei $A_S(N_S, Z_S)$ of the sample (see Fig. 1), induces the photonuclear reactions

$$\gamma + A_S(Z_S, N_S) \Longrightarrow A'_S(Z_S, N_S - 1) + n,$$

$$\begin{gathered}\gamma + A_S(Z_S, N_S) \Longrightarrow A'_S(Z_S - 1, N_S - 1) + n + p, \\ \gamma + A_S(Z_S, N_S) \Longrightarrow A'_S(Z_S, N_S - 2) + 2n, \\ \gamma + A_S(Z_S, N_S) \Longrightarrow A'_S(Z_S, N_S - 3) + 3n, \\ \dots \\ \gamma + A_S(Z_S, N_S) \Longrightarrow \text{fission fragments} + \nu_{\gamma nF}\ \text{fission neutrons},\end{gathered} \tag{2.2}$$

with the cross sections $\sigma_{\gamma n}, \sigma_{\gamma np}, \sigma_{\gamma 2n}, \sigma_{\gamma 3n}, \sigma_{\gamma F}$, etc., to yield neutrons. Certainly, these processes (2.2) can only be realized, when the energy E_γ of γ rays is, at least, greater than the neutron binding energy B_n and the fission threshold energy B_F of a considered nucleus $A_S(Z_S, N_S)$, $E_\gamma > B_n, B_F$. Actually, these processes will successfully run provided E_γ is of the order of, and comes over the energy E_{GR} of giant resonance in the photonuclear reactions on respective nuclei, $E_\gamma \gtrsim E_{GR}(Z, N) \sim$ 10–17 MeV [10]. As a matter of course, an electron must have got the energy $E_e > E_\gamma$ in order to give birth to the bremsstrahlung with the required energy E_γ. Thus, only the processes involving the electron and photon energies

$$E_\gamma, E_e \gtrsim E_{GR} \tag{2.3}$$

are to be taken into consideration and explored, which is the key point of our treatment. Next, we limit the current study by the condition

$$E_e \leqslant 100\ \text{MeV} \tag{2.4}$$

as well. The guide relations (2.3), (2.4) govern all the presented calculations, specifying the energy area where our consideration holds true. Also, in the ordinary way, all the evaluations we make in the work are the first α-order, and we abandon contributions from all the high α-order processes. The direct nuclear reactions, including neutron production, induced by electrons are left out as well. The direct production of neutrons by electrons is about two orders of magnitude smaller than the neutron production by high energy photons [10].

Let an electron with energy $E_e(x)$ be scattered by an atom at a point x, see Fig. 1. Manifold reactions hold thereby, in particular the bremsstrahlung with various momenta. Yet we are only to treat the high-energy γ radiation which can serve to induce reactions (2.2).

As the relation (2.3) holds, for all the processes we are interested in, the angular distribution of scattered electrons as well as emitted photons has got a sharp maximum in momentum direction of an initial electron. Both electrons and

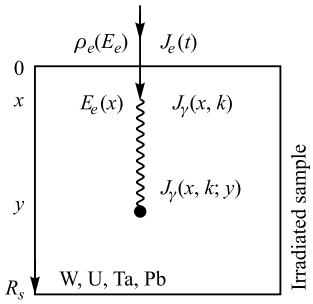

Fig. 1. The scheme of neutron yield by electron beam

photons spread within a small, rather negligible, solid angle $\Theta \sim m/E_e$ around direction of the initial electron momentum [11–13].

The electron scattering in field of atomic nucleus is known to be of primary importence. With proper allowance for screening, upon integrating the bremsstrahlung cross section over the angle between the momenta of incident electron and emitted photon, the very handy expression for the cross section to describe the photon energy distribution results as follows (see, e.g., [12, 14, 15]):

$$\frac{\mathrm{d}\,\sigma_{bS}(k, E_e(x))}{\mathrm{d}\,k} = \frac{2Z_S^2}{137} r_0^2 \frac{1}{k} \times$$
$$\times \left\{ \left(\frac{E_e^2(x) + {E'_e}^2(x)}{E_e^2(x)} - \frac{2E'_e(x)}{3E_e(x)} \right) \cdot \left(\ln M + 1 - \frac{2}{b} \arctan b \right) + \right.$$
$$\left. + \frac{E'_e(x)}{E_e(x)} \left(\frac{2}{b^2} \ln(1 + b^2) + \frac{4(2 - b^2)}{3b^3} \arctan b - \frac{8}{3b^2} + \frac{2}{9} \right) \right\}, \quad (2.5)$$

where $k = E_\gamma$ stands for the energy of radiated γ-quantum; $E_e(x)$ is electron energy at a point x, $E'_e(x) = E_e(x) - k \gtrsim m$; Z_S is the atomic number of the sample material, and

$$b = \frac{2E_e E'_E Z^{1/3}}{C\,m\,k}, \quad \frac{1}{M} = \left(\frac{m\,k}{2E_e E'_e} \right)^2 + \frac{Z_S^{2/3}}{C^2},$$
$$C = 111, \quad r_0 = \frac{e^2}{m} = 2.818 \cdot 10^{-13} \text{ cm}.$$

Besides this high energy bremsstrahlung in the field of nucleus (2.5), there exists one by scattering an incident electron by atomic electrons. For a fast electron, $E_e \gg m$, the cross section of this process is known to coincide with the bremsstrahlung cross section on nucleus with $Z = 1$ [11–13]. Then, the atomic electrons contribution into the whole electron bremsstrahlung is taken into account just by replacing the factor Z_S^2 in Eq. (2.5) by $Z_S(Z_S + \delta)$ with $\delta \lesssim 1$. As for heavy sample atoms $Z_S \gg 1$, this correction is rather of very small value, though taken into account.

The bremsstrahlung (2.5) of an electron at a distance x from starting edge of sample is determined by the electron energy $E_e(x)$, that is what we are now to acquire.

In passing across a sample, a high energy electron is primarily known to lose its energy (see, e.g., [11–13]) due to the bremsstrahlung by scattering in fields of heavy atoms of a sample. So far $E_e \gg m$, the scattering angle $\Theta \lesssim m/E_e \ll 1$ is understood to be rather negligible. The bremsstrahlung, with all the feasible energies $k = E_\gamma$, causes the mean energy loss of electron on a unit of path [11,12]

$$-\frac{\mathrm{d}\,E_e(x)}{\mathrm{d}x} = \mathcal{N}_S E_e(x) \varphi_{\mathrm{rad}}(E_e). \quad (2.6)$$

The number $\mathcal{N}_S$ of scattering atoms of sample in 1 cm^3 is

$$\mathcal{N}_S = \frac{\rho_S \cdot 6.022 \cdot 10^{23}}{A_S}, \tag{2.7}$$

where ρ_S is the sample material density, and A_S is its atomic weight. The quantity $\varphi_{\rm rad}$ is written in the form

$$\varphi_{\rm rad} = \bar{\varphi} \cdot K_S(E_e) = K_S(E_e) Z_S^2 \cdot 5.795 \cdot 10^{-28}\ \text{cm}^2. \tag{2.8}$$

The coefficient K_S, very slightly varying with energy E_e, provided $E_e \gtrsim 10$ MeV, can be found in [11, 12, 16] for various heavy atoms. So, upon passing a distance x, an electron with the initial energy $E_e(0)$ will have got, in consequence of the radiative losses, the energy

$$E_{e\,\rm rad}(x) \approx E_e(0) \exp\left[-x\mathcal{N}_S\varphi_{\rm rad}\right]. \tag{2.9}$$

In fast electrons, $E_e \gg m$, elastic scattering on heavy nuclei of a sample material, the angular distribution has got a very sharp maximum, within the solid angle $\Theta < (m/E_e)^2$, and therefore can be left out of our consideration [11–13].

In treating a fast electron collision with atomic electrons, without photon emitting, we are to consider two cases. Firstly, let the momentum Δ_I transferred to an atomic electron be

$$\Delta_I \lesssim I_Z \approx 13.5 Z_S\ \text{eV}, \tag{2.10}$$

the ionization potential of atom. Apparently, as $\Delta_I \ll E_e$, the scattering angle is negligible. The mean electron energy loss on a unit of path, caused by its inelastic collisions with atoms, is described by the expression (see [11, 12, 14])

$$-\frac{{\rm d}E_e(x)}{{\rm d}x} = 2\pi r_0^2 m \mathcal{N}_S Z_S \ln\frac{E_e^3(x)}{2mI_Z^2}, \tag{2.11}$$

which can be rewritten in the form

$$x = -\frac{1}{6\pi r_0^2 m \mathcal{N}_S Z_S} \int\limits_{E_e(0)}^{E_{e\,I}(x)} \frac{{\rm d}E}{\ln[E(2mI_Z^2)^{-1/3}]}, \tag{2.12}$$

where $E_e(0)$ is the electron energy at the starting edge of an irradiated sample, and $E_{e\,I}(x)$ stands for the electron energy upon passing the distance x, caused by the ionization losses. With the conditions (2.3), (2.4), we can actually presume:

$$\ln E \approx \ln E_e^{\rm av}, \quad E_e^{\rm av} = \frac{E_e(0) + E_{GR}}{2} \tag{2.13}$$

in Eq. (2.12). Then we arrive at the estimation of the electron energy loss on the distance x due to the inelastic electron collisions with atoms

$$\Delta E_{e\,I}(x) \approx -x6\pi r_0^2 m\mathcal{N}_S Z_S \ln[E_e^{\rm av}(2mI_Z^2)^{-1/3}]. \qquad (2.14)$$

Secondly, when, unlike (2.10), the momentum transferred $\Delta_I \gg I_Z$, yet still $\Delta_I \ll E_e$ anyway, atomic electrons can be considered as free ones, and the fast electron interaction reduces to the elastic forward scattering on free resting electrons [11, 13], which causes no energy loss, as a matter of fact.

Amenably to Eqs. (2.6), (2.9), (2.11)–(2.14), an electron with the incident energy $E_e(0)$ at the starting edge of a sample has got the energy

$$E_e(x) \approx E_{e\,\rm rad}(x) - \frac{6\pi r_0^2 m Z_C \ln[E_e^{\rm av}(2mI_Z^2)^{-1/3}]}{\varphi_{\rm rad}} \left(1 - \frac{E_{e\,\rm rad}(x)}{E_e(0)}\right) \approx$$
$$\approx E_{e\,\rm rad}(x) + \Delta E_{e\,I}(x), \quad (2.15)$$

upon passing the path x through sample (see Fig. 1). Our consideration holds only until the electron energy satisfies the key constraint (2.3), so that electron can serve to induce the reactions (2.2). Yet we need not take care of correct describing interactions of both electrons and photons, when their energies do not satisfy the condition (2.3).

Just the x-dependent energy $E_e(x)$ (2.15) is to be substituted into Eq. (2.5) to describe the bremsstrahlung of an electron at the distance x from the starting edge of an irradiated sample (see Fig. 1). Thus, the high energy bremsstrahlung production cross section (2.5) turns out to be function of the distance x, via the electron energy $E_e(x)$ (2.15).

Let us stress ones again that besides the bremsstrahlung discussed just above, there exists the γ radiation of electrons with energies beyond the key constraint (2.3). Of course, the energy and angular distribution of this γ radiation cannot be considered so plainly as it was done in the presented work. Yet such γ rays do not induce the desirable processes (2.2). As understood, so far the relations (2.3), (2.4) hold, we carry out consistently all our plain calculations, without having any recourse to the so-called «Monte Carlo simulation», the sufficient accuracy $\sim$ 10–20% is provided thereby.

3. BREMSSTRAHLUNG PASSING THROUGH SAMPLE

As expounded above, only the bremsstrahlung with $k \gtrsim 10$ MeV $\gg m$, described by Eq. (2.5), is of value to induce the desirable photonuclear reactions (2.2). This bremsstrahlung, caused by the initial electron beam with the energy E_e and the current density $J_e(t)$, when stems at a distance x from the

starting edge of an irradiated sample, is described by the photon current density (2.1)

$$J_{S\gamma}(x,k,E_e,Z_S,\rho_S,t)=J_e(t)\mathcal{N}_S\frac{\mathrm{d}\,\sigma_{Sb}(k,E_e(x))}{\mathrm{d}k}, \tag{3.1}$$

where the cross section $\mathrm{d}\,\sigma_{bS}(k,E_e(x))/\mathrm{d}\,k$ is given by Eq. (2.5) with the electron energy $E_e(x)$ (2.15).

This γ flux spreads forward, inducing the photonuclear reactions (2.2). In bremsstrahlung passing the distance $(y-x)$ from a point x up to a point y, where neutron generating occurs (see Fig. 1), there are three processes which cause the continuing γ-ray absorption [11–13]: 1) the e^+e^--pair production; 2) the photoeffect; 3) the Compton scattering on electrons, the first one is known to be of crucial importance at the considered $k\gtrsim 10$ MeV [11–13]. Consequently, the bremsstrahlung current density $J_\gamma(x,k)$ (3.1) decreases, becoming at a point $y\geqslant x$

$$J_{S\gamma}(x,k,E_e,Z_S,\rho_S,t;y)=J_{S\gamma}(x,k,E_e,Z_S,\rho_S,t)\exp\left(-\frac{y-x}{l_S(Z_S,\mathcal{N}_S,k,\rho_S)}\right), \tag{3.2}$$

where the length of absorption l consists from three aforesaid parts

$$\frac{1}{l_S}=\frac{1}{l_{\mathrm{pair}}}+\frac{1}{l_{\mathrm{photo}}}+\frac{1}{l_{\mathrm{Comp}}}. \tag{3.3}$$

Generally speaking, a tiny small quantity $1/l_{\gamma n}$, caused by the reactions like (2.2), should have been added to right-hand side of Eq. (3.3), for conscience's sake. The values of l for various materials are found, for instance, in [12,16]. Let us mention that we deal with the γ-ray energies just above the so-called «area of maximum transparency» [11, 12, 16].

Upon integrating the expression (3.2) over x up to y, we would obtain the γ flux

$$J_{S\gamma}(k,E_e,Z_S,\rho_S,t;y)=\int\limits_0^y \mathrm{d}x J_{S\gamma}(x,k,E_e,Z_S,\rho_S,t;y) \tag{3.4}$$

at a distance y from the initial edge of sample. As plain evaluation proves, this quantity firstly increases with y growth, gets its maximum at $y_{\max}(E_e)$, and then falls down, tending to zero. In Fig. 2, as an example, we display k-dependence of the γ flux (3.4) for tungsten sample at the distances $y_{\max}$ at which $J_{W\gamma}(k,E_e,Z_S,\rho_S,t;y)$ gets its maximum for a given electron energy E_e.

As understood, precision of all the carried out calculations is proved to be at least of the order $\sim\dfrac{m}{E_{GR}}$, $\sim\dfrac{I_Z}{E_{GR}}$, that is anyway none the worse than $\sim 10\%$.

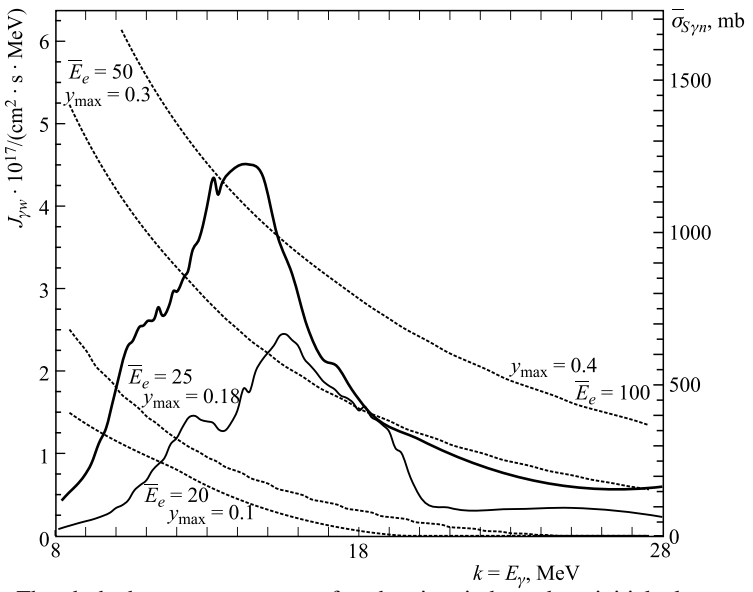

Fig. 2. The dashed curves represent, for the time-independent initial electron current density $J_e = 1\ \mathrm{A/cm}^2$ and various energies $\bar{E}_e$ (MeV) (4.3), the k-dependence of the γ flux (3.4), in a tungsten sample, at $y = y_{\max}$ (cm) where this quantity $J_{W\gamma}(k; y)$ (3.4) gets its maximum. The values of $y_{\max}$ and $\bar{E}_e$ are plotted along the corresponding curves. The solid curves represent the k-dependence of the cross sections (4.2) $\bar{\sigma}_{S\gamma n}(k)$, the thick line for uranium, $S = {}^{238}\mathrm{U}$ [19], and the thin line for tungsten, $S = {}^{184}\mathrm{W}$ [18], samples, respectively

With taken into consideration the restrictions imposed by the guide conditions (2.3), (2.4), we shall now discuss how the cascade of electrons and photons, practicable to the neutron production (2.2), would emerge. The processes in that an electron with the energy $E_e < E_{GR}$ participates cannot anyway lead to any discernible contribution into the photo-neutron production (2.2). In slowing-down from the initial energy $E_e(0)$ to the energy E_{GR}, an electron loses the energy

$$\tilde{\Delta} \approx E_e(0) - E_{GR}. \tag{3.5}$$

This energy loss $\tilde{\Delta}$ itself is not considered to be small. So, at the maxima currently treated electron energy $E_e(0) = 100$ MeV, we would have got $\tilde{\Delta} \approx 85$ MeV, and for the timely most vital $E_e(0) = 50$ MeV we would arrive at $\tilde{\Delta} \approx 35$ MeV. As generally received [12, 17], the primary share of this energy loss $\tilde{\Delta}$ is radiated most probably as the γ rays with energies

$$\tilde{k} = \tilde{E}\gamma \approx \frac{\tilde{\Delta}}{2}. \tag{3.6}$$

Only a small part of this energy loss $\tilde{\Delta}$ is emitted as a flux of comparatively soft photons, and γ radiating with the energies $k = E_\gamma > \tilde{k}$ proves to be all the more negligible [12, 17]. As was already discussed above, in absorbing a photon with the considerable energy $\tilde{k}$ (3.6), the e^+e^- pairs are produced with approximately equal energies

$$E^+ \approx E^- \approx \frac{\tilde{k}}{2} \approx \frac{\tilde{\Delta}}{4}. \tag{3.7}$$

Surely, there is no reason to suggest these energies to be as small as negligible, yet, anyway, they are nevertheless substantially smaller than the initial electron energy $E_e(0)$. Thus for the timely most vital case $E_e(0) = 50$ MeV, we have got $E^\pm \approx 8$ MeV $< E_{GR}$, so that the thereby produced e^+, e^- can never contribute to the neutron production (2.2) at all, which is understood in observing Fig. 2. Put another way, there would be a cascade, but the particles participating therein would have got energies beyond the key condition (2.3). Notwithstanding, at the largest initial electron energy we currently consider (2.4), $E_e(0) \sim 100$ MeV, there would be $E^\pm \sim 20$ MeV, so as, generally speaking, these e^+, e^- themselves would give birth to the bremsstrahlung which could in turn serve to the photo-neutron production (2.2). Yet being, strictly speaking, not negligible, the neutron production, caused by those secondary electrons with energies $E^\pm \sim 20$ MeV, is anyway noticeably smaller than the neutron production due to the initial electrons with $E_e(0) \sim 100$ MeV. Thus, when we abandon the above explicated cascade, the thereby inherent ambiguities will never come over $\sim 30\%$, even at $E_e(0) \sim 100$ MeV, whereas at $E_e(0) \lesssim 50$ MeV our approach holds apparently true with accuracy $\sim 10\%$. That is why we do not draw into consideration the bremsstrahlung which would be induced by the electrons which themselves would be originated by absorption of the bremsstrahlung, which in its turn is due to scattering an initial electron on nuclei in irradiated sample. Yet, as understood, when the initial electron energy were appreciably atop the constraint (2.4), the developed approach would not be valid.

4. PRODUCING NEUTRONS BY γ FLUX

The rate of neutron production, which is caused by the processes (2.2) at a point y (see Fig. 1) by the γ flux originated at a point x, proves to be

$$\frac{\mathrm{d}n_{Sn}(x,k,y,E_e;t)}{\mathrm{d}t} = \mathcal{N}_S \cdot \bar{\sigma}_{S\gamma n}(k) \cdot J_{S\gamma}(x,k,E_e,Z_S,\rho_S,t;y), \tag{4.1}$$

where the quantity

$$\bar{\sigma}_{S\gamma n}(k) = \sigma_{S\gamma n}(k) + 2\sigma_{S\gamma 2n}(k) + \sigma_{S\gamma np}(k) + 3\sigma_{S\gamma 3n}(k) + \ldots$$
$$\ldots + \nu_{\gamma nF} \cdot \sigma_{S\gamma F}(k) = \nu_{S\gamma nt}(k) \cdot \sigma_{S\gamma nt}(k) \tag{4.2}$$

stands for the total cross section of neutron production in the processes (2.2), which are known to be primary due to the giant resonance in the nuclear photoabsorption [10].

Surely, the electron energy distribution $\rho_e(E)$ of a real electron beam of e-linac cannot be merely δ function. In our actual evaluation, we choose the electron density distribution in the form

$$\rho_e(E) = \frac{1}{n}\exp\left[-((E-\bar{E})/\Delta_e)^2\right], \quad \bar{E} = \frac{E_e^b + E_e^u}{2}, \tag{4.3}$$

$$1 = \int\limits_{E_e^b}^{E_e^u} \mathrm{d}E \rho_e(E),$$

where E_e^b and E_e^u stand for the bottom and upper limits of electron energy in a beam. Surely, when $\Delta_e \to 0$, Eq. (4.3) reduces to the δ-function electron energy distribution. Also, let us recall the initial electron current density J_e in Eqs. (3.1), (4.1) is given in $\mathrm{A/cm^2} = 10^{19}\mathrm{e^-}/(1.602 \cdot \mathrm{s} \cdot \mathrm{cm^2})$, where $\mathrm{e^-}$ is the electron electric charge.

Upon proper integrating expression (4.1) over the variables x, y, the initial electron energy E, and the photon energy k, we arrive at the neutron production rate, the number of neutrons generated per 1 s, inside the irradiated sample, the neutron radiator, with longitudinal size R_S, per 1 $\mathrm{cm^2}$ of sample area,

$$Y_S(E_e^b, E_e^u, \Delta_e, R_S; t) = \frac{\mathrm{d}\,\bar{n}_{Sn}(E_e^b, E_e^u, \Delta_e, R_S; t)}{\mathrm{d}\,t} =$$

$$= J_e(t) \cdot \mathcal{N}_S^2 \int\limits_0^{R_S} \mathrm{d}\,x \int\limits_0^{\infty} \mathrm{d}\,k \cdot l_S(k) \cdot \bar{\sigma}_{S\gamma n}(k) \times$$

$$\times \left(1 - \exp\left[(x - R_S)/l_S(k)\right]\right) \int\limits_{E_e^b}^{E_e^u} \mathrm{d}\,E \rho_e(E) \frac{\mathrm{d}\,\sigma_{Sb}(k, E_e(x))}{\mathrm{d}\,k}. \tag{4.4}$$

Certainly, substantial contribution into the integration over photon energy k stems from the area where the product

$$\left(\frac{\mathrm{d}\,\sigma_b S(k, E_e(x))}{\mathrm{d}\,k}\right) \cdot \bar{\sigma}_{S\gamma\, n}(k) \tag{4.5}$$

has got its greatest value, i.e., from area of the giant resonance, which comes to light in observing Fig. 2. The presented picture typifies the treatment of neutron production by means of electron beam. Beyond any questions, the values

$k \lesssim B_n, B_{\gamma F}$ and $k \gtrsim E_e$ contribute just nothing into this integral over k into Eq. (4.4).

By now, there exist high precision reliable measurements of the cross sections (4.2) with photon energies k within the giant resonance area for manifold nuclei, see, for instance, [18–21]. The respective data are put to use in our evaluations what follow (see Sec. 5). The errors in these $\bar{\sigma}_{S\gamma n}(k)$ measurements may rather amount $\sim 10\%$, which puts a bound to the accuracy attainable in our calculations. It is to point out that at the large enough converted γ-ray energies, $k = E_\gamma \gtrsim 25$ MeV, the contribution to (4.4) from area beyond the giant-resonance nuclear photoabsorption is discernible because there exists at these energies the nuclear photoabsorption due to the surface absorption, the virtual quasi-deuteron absorption, and the absorption caused by the nucleon polarizability in nucleus [22]. The respective measurements of the neutron production cross section (4.2) were carried out and discussed in a number of investigations [23–25], with a special care paid to determine the total neutron multiplicity at such a large photon energy $k \gtrsim 25$ MeV, the large enough value $\nu_{S\gamma nt}(k) \sim 10$ found therewith. This high energy photons contribution in the neutron yield (4.4) is also taken into account in the computations what follow (see Sec. 5), though its impact onto the quantities we have been considering proves to be never more than $\sim 30\%$, even at $E_e(0) \sim 100$ MeV.

As realized, expression (4.4) describes the total neutron yield caused immediately by the photonuclear reactions (2.2), leaving out the treatment of the neutron energy distribution. This first generation neutrons, traveling through sample before living it, interact with nuclei of sample, which results in modification of the original neutron flux. To realize how significant these modifications could be we are to asses the quantity

$$c = 1 - \exp\left[-\kappa\right] \quad \text{with} \quad \kappa = \bar{\sigma}_{Sn}(\bar{\epsilon})\bar{L}\mathcal{N}_S. \tag{4.6}$$

Here the mean energy of neutrons produced in reactions (2.2) is certain to be $\bar{\epsilon} \sim 1$ MeV. The manifold processes contribute to the mean cross section $\bar{\sigma}_{Sn}(\bar{\epsilon})$ of neutron interaction with sample nuclei. Among these, the reactions $A(Z,N)(n\gamma)A'(Z,N+1)$ and $A(Z,N)$ (*n fission fragments*) ν *neutrons* immediately cause the total neutron flux modification. As known, the cross sections of these reactions at $\bar{\epsilon} \sim 1$ MeV are estimated to be never more than $\sigma_{n\gamma}(\bar{\epsilon}) \lesssim 1$ b, $\sigma_{nF}(\bar{\epsilon}) \lesssim 1$ b for any heavy nuclei, like U, Ta, W, Pb, see [19, 26–28]. The obvious estimation $\bar{L} < 1$ cm is understood for a mean path covered by neutron until leaving a sample with the size $R_S < 10$ cm and 1 cm^2 area. Then, with $\mathcal{N}_S$ (2.7), the plausible estimations hold

$$\kappa \lesssim 0.1, \quad c \lesssim 0.1, \tag{4.7}$$

so that the aforesaid modifications of neutron flux Y_S (4.4) can be left out, at least at this stage of neutron yield treatment, with a sufficient accuracy $\sim 10\%$. Yet

careful study of neutron energy distribution is certain to be needful for various applications of the produced neutrons, and this is what we are on the point of treating in an ensuing work.

5. COMPUTATION FINDINGS

To acquire e-linac-driven neutron producing, the numerical computation is carried out with the most practicable irradiated samples: tantalum, uranium, tungsten and lead.

In all the evaluations what follow we utilize the data on the cross sections $\bar{\sigma}_{S\gamma n}$ (4.2) at $k = E_\gamma \sim 5$–25 MeV, the area of GR energy, obtained in investigations [18–21] for tungsten, uranium, lead and tantalum, respectively. For energy $k = E_\gamma \sim 25$–100 MeV, atop GR energy, we put to use the $\bar{\sigma}_{S\gamma n}$ data acquired in [23–25]. Thus, all our computations are completely based upon the results of experimental measurements of $\bar{\sigma}_{S\gamma n}$ (4.2), so that were those data precarious or not intelligible, the results we have gained would be wrong.

To start with, we have learnt how the neutron yield (4.4) does depend on the sample size R_S for various sample materials. As one concludes in observing Table 1, there is quick saturation of Y_S as function on R_S, so that there sees no reason to choose $R_S > 4$ cm. The explicated R_S dependence of Y_S holds for any treated electron energies.

Table 1. The yield of neutrons $Y_S[10^{11}/\mathrm{s}]$ in tungsten, $S =$ W, in uranium, $S =$ U, and in lead, $S =$ Pb samples, with the size $R_S = R$ [cm] and 1 cm^2 area, irradiated by constant electron current of density $J_e = 10^{-5}$ A/cm^2, with the parameters $\bar{E}_e = 30$ MeV, $E_e^b = 29$ MeV, $E_e^u = 31$ MeV, $\Delta_e = 0.2$ MeV of the electron energy distribution $\rho_e(E)$ (4.3)

R_S	0.1	1.0	2.0	3.0	4.0	5.0	6.0
$Y_{^{\mathrm{nat}}\mathrm{W}}$	0.11	2.14	2.91	3.19	3.30	3.33	3.35
$Y_{^{238}\mathrm{U}}$	0.26	4.83	6.52	7.12	7.35	7.43	7.46
$Y_{^{208}\mathrm{Pb}}$	0.05	1.95	3.14	3.82	4.21	4.44	4.57

A superfluous R_S value would merely lead to undesirable additional heating of sample. An excessive size R_S is not only useless, but would cause considerable complications to design, construct, and operate a respective neutron source. In particular, the issue of cooling installation would call for a special additional care. Certainly, we are anyway to deal with the case that the sample area fits to, or is only a bit greater than the area of electron beam irradiating a sample. So, all beam electrons are to be engaged on neutron producing, yet there should actually be no useless sample material.

The dependence of neutron yield on electron energy is understood with observing the results presented in Table 2. As seen, augmentation of electron energy causes neutron yield growth which shows up apparently to be not uniform. Increase of electron energy from $\bar{E}_e = 20$ MeV up to $\bar{E}_e = 50$ MeV enhances neutron yield by about a factor of five–seven, whereas the electron energy growth from $\bar{E}_e = 50$ MeV to $\bar{E}_e = 100$ MeV results in less than a double increase of the neutron yield. So, the energy $\bar{E}_e = 50$ Mev can be thought to be the most eligible, as substantial technical challenges would emerge when electron energy became as large as $\gtrsim 100$ MeV. Thus, keeping minimum power $W = E_e J_e$ increase, it is more profitable to enhance E_e until $E_e < 50$ MeV, yet at $E_e \gtrsim 50$ MeV, enhancement of the initial electron current J_e turns out to be preferable. Surely, these inferences apply to any samples.

Table 2. The yield of neutrons $Y_S[10^{11}/\mathrm{s}]$ in tantalum, $S =$ Ta, in tungsten, $S =$ W, in uranium, $S =$ U, and in lead, $S =$ Pb, samples, with the size $R_S = 3$ cm and 1 cm^2 area, irradiated by the constant electron density current $J_e = 10^{-5}$ A/cm^2, with various parameters $\bar{E}_e, E_e^b, E_e^u, \Delta_e$ (all in MeV) of the electron energy distribution $\rho_e(E)$ (4.3)

$\bar{E}_e$	20.0	22.0	25.0	30.0	40.0	50.0	100.0
E_e^u	20.5	22.5	25.5	31.0	41.5	52.5	105.0
E_e^b	19.5	21.5	24.5	29.0	38.5	47.5	95.0
Δ_e	0.2	0.2	0.2	0.2	0.5	0.5	1.0
$Y_{^{181}\mathrm{Ta}}$	0.85	1.2	1.74	2.63	4.28	5.73	11.34
$Y_{^{\mathrm{nat}}\mathrm{W}}$	0.94	1.39	2.08	3.19	5.14	6.80	12.80
$Y_{^{238}\mathrm{U}}$	2.51	3.42	4.80	7.12	11.41	15.07	28.94
$Y_{^{208}\mathrm{Pb}}$	1.32	1.81	2.57	3.82	6.10	8.10	15.26

As realized from the data presented in the Tables, the neutron yield Y_{U} in an uranium sample is about twice that the yield Y_{W} in a tungsten sample, under equal conditions. This comes easily to light in observing the curves in Fig. 2, presenting the cross sections of the photonuclear neutron production on tungsten and uranium samples, as the quantity $\bar{\sigma}_{U\gamma n}(k)$ shows up to come substantially before $\bar{\sigma}_{\mathrm{W}\gamma n}(k)$. Of course, the discernible differences between the quantities $\mathrm{d}\,\sigma_{b\mathrm{U}}/\mathrm{d}\,k, l_{\mathrm{U}}, \mathcal{N}_{\mathrm{U}}, K_{\mathrm{U}}$ and $\mathrm{d}\,\sigma_{b\mathrm{W}}/\mathrm{d}\,k, l_{\mathrm{W}}, \mathcal{N}_{\mathrm{W}}, K_{\mathrm{W}}$ (see Eqs. (2.5), (2.7), (2.8)) are also a reason to the difference between Y_{U} and Y_{W}. The difference between the yields Y_{W} and Y_{Ta} for tungsten and tantalum may be said to be rather negligible. Thus, as neutron yield doubling is considered to be of substantial value, an uranium sample is to be used.

Now the point is to correlate the computed yields Y_{comp} with the $Y_{\text{«exp»}}$ what were ascertained in exploiting the various e-linac-driven neutron sources, both the modern, like GELINA [29], ELBE [30], POHANG [31], IREN [9], and some obsolete ones, like the sources in RPI, LLL [32]. The respective correlation

is presented by Table 3. Of course, one must keep in mind that accuracy of the presented calculations is ~ 10–20%, and the appropriate experimental errors ought to be prescribed to the $Y_{\text{«exp»}}$ values as well. We are writing the lower index «exp» within quotation marks to emphasize that in obtaining these values $Y_{\text{«exp»}}$ some «numerical simulations» could be used. Surely, in any cases the irradiated sample is taken for granted to be adjusted so that electron beam would completely engaged on sample irradiating, as discussed above. Certainly, it is to understand these Y_{comp} are determined by the average electron current provided by the respective e-linac. For the general comprehension's sake, Table 3 offers the maximum pulse repetition frequency (p.r.f.) and the minimum pulse width (p.w.) of electron beam which can be provided by the respective facility.

Table 3. For the various e-linac-driven neutron sources, the «experimental», $Y_{\text{«exp»}}[10^{11}/\text{s}]$, and computed in the present work, $Y_{\text{comp}}[10^{11}/\text{s}]$, neutron yields are given for the various samples (the second row) with the longitudinal sizes R_S [cm], irradiated by the total average electron current $\bar{J}_e$ [A10^{-5}] with the mean electron energy $\bar{E}_e$ [MeV]. The maximum pulse repetition frequency (p.r.f.) [kHz] and the minimum pulse width (p.w.) [ns], attainable at the respective facilities, are displayed in the sixth and seventh rows, respectively

Institute Facility	IRMM GELINA	FZR ELBE	POHANG LINAC	JINR IREN	RPI LINAC	LLNL LIVERMORE
Sample	^{238}U	^{208}Pb	^{181}Ta	$^{\text{nat}}$W	^{181}Ta	^{181}Ta
R_S	$\gtrsim 4.0^a$	1.12^b	$\sim 8.0^c$	10.0^d	$\sim 5.0^e$	$\sim 5.0^e$
$\bar{J}_e$	10^a	100^b	0.072^c	0.5^d	0.72^e	7.2^e
$\bar{E}_e$	100^a	30^b	75^c	30^d	80^e	115^e
p.r.f.	0.8^a	500^b	0.012^c	0.025^d	0.72^e	1.44^e
p.w.	0.67^a	0.005^b	1500^c	100^d	10^e	5^e
$Y_{\text{«exp»}}$	340^a	190^b	1.0^c	0.3–0.5^d	11^e	140^e
Y_{comp}	300	195	0.75	1.66	8.5	100

[a] The data from [29].
[b] The data from [30].
[c] The data from [31].
[d] The data from [9].
[e] The data from [32].

As was already explicated, all our computations are essentially determined by the data of experimental measurements of cross sections (4.2). For all the considered samples but lead, using of any by now published $\bar{\sigma}_{S\gamma n}$ values, the results of computation do actually coincide. Yet for lead sample, usage of the data offered in [20] and in [33] procures the rather different outcomes, as one can grasp from what is displayed in Table 4.

Table 4. The neutron yields in a lead sample with the size $R_{\text{Pb}} = 1.12$ cm irradiated by the average total electron current $\bar{J}_e = 1$ mA with the various electron mean energies $\bar{E}_e$ [MeV], computed utilizing $\bar{\sigma}_{\gamma n}$ from [20], $Y[10^{11}/\text{s}]$, and from [33], $Y^*[10^{11}/\text{s}]$, along with the corresponding «experimental» yields $Y_{\text{«exp»}}[10^{11}/\text{s}]$ from [30]

$\bar{E}_e$	Y	Y^*	$Y_{\text{«exp»}}$
20	70	40	79
30	195	111	190
40	299	179	279

Let us point out that a particular caution must be exercised in interpretation of the Y_{comp} computed at electron energy $\bar{E}_e \gtrsim 100$ MeV, and in discussing the correlation between Y_{comp} and $Y_{\text{«exp»}}$ at such electron energies. We have to keep in mind that our calculation, as was explicated above, Sec. 3, does not allow for occurrence of the cascade of e^+e^- pairs and γ rays, which is thought to be of value at energies $\bar{E}_e \gtrsim 100$ MeV. That is why there is no wonder that the calculated neutron yields Y_{comp} show up to be rather appreciably smaller than the corresponding $Y_{\text{«exp»}}$ at such electron energies. In this respect, we do not as well afford to discuss the neutron yield at the facilities, e.g., ORELA [6], that operate with too high initial electron energy, $E_e \sim 200$ MeV.

Thus, our findings assort well with the data gained in all the investigations, but the work [9]. Analyzing contents of Tables 1–3, one infers that the data asserted at IREN (JINR) [9] turn out to be rather incompatible with all other nowadays existing observations. Upon careful inquiring into what is offered in the work [9], there sees no intelligible resolution of this issue.

Let us emphasize that the plain findings of our inquiry are purely based on the quantum electrodynamics, nuclear physics and the quite reliable experimental data, nothing else. There sees no need for having any recourse to the so-called «numerical Monte Carlo simulation». As was seen, our strait physical treatment is quite visible, as against the extremely complex and rather vague Monte Carlo simulation.

After all, we become convinced that the presented approach is reliable and can be of use for currently ongoing investigation of the e-linac-driven neutron sources.

Acknowledgements. Authors are thankful to Z. Panteleev, P. Sedishev for the valuable discussions.

REFERENCES

1. NEANDC Monograph Ser. Neutron Phys. and Nucl. Data in Science and Technology. V. 2. Neutron Sources for Basic Phys. and Appl. / Ed. by S. Cierjacks. Vienna: NEANDC, 1983.
2. *Carpenter J. M.* // NIM. 1977. V. 145. P. 91.

3. *Andriamonje S. et al.* Neutron TOF Facility (PS 213). Technical Design Report, CERN/INTC/2000-004, 2000.
4. *Schweiner G. W.* // Nucl. Phys. A. 1967. V. 100. P. 537;
Cierjacks S. et al. // Review of Scientific Instruments. 1968. V. 39. P. 1279.
5. *Bensussan A., Salome J. M.* // NIM. 1978. V. 155. P. 11.
6. *Bigelow T. S. et al.* // Proc. of LINAC 2006, Knoxville, Tennessee, USA (ORNL, Oak Ridge, TN 37830, USA, 2007). P. 79.
7. *Barschall H. H.* // An. Rev. Nucl. Particle Science, 1978;
Barschall H. H. Saclay Rep. CEA-R-4838. 1974. P. 56.
8. *Frank I. M.* // Particles and Nucleus. 1972. V. 2. P. 805.
9. *Belicov O. V. et al.* // Journal of Phys.: Conference Series. 2010. V. 205. P. 012053.
10. Landolt–Börnstein Database. Elementary Particles, Nuclei and Atoms. A. V. 16 / Ed. by H. Shopper. Springer, 2000.
11. *Akhiezer A. I., Berestetskii V. B.* Quantum Electrodynamics. M.: FM, 1959.
12. *Heitler W.* The Quantum Theory of Radiation. Oxford; London: Clarendon Press, 1954.
13. *Berestetskii V. B., Lifshits E. M., Pitaevskii L. P.* Relativistic Quantum Theory. Oxford: Pergamon, 1971.
14. *Bethe H., Heitler W.* // Proc. Roy. Soc. A. 1934. V. 146. P. 83.
15. *Shiff L. I.* // Phys. Rev. 1951. V. 83. P. 252.
16. The Nuclear Handbook / Ed. by O. R. Frisch. London: George Newnes Limited, 1958;
The Tables of Physical Quantities / Ed. by I. K. Kikoin. M.: Atomizdat, 1976.
17. *Carlson J. F., Oppenheimer J. R.* // Phys. Rev. 1936. V. 51. P. 220;
Bhabha H. J., Heitler W. // Proc. Roy. Soc. A. 1936. V. 159. P. 432;
Jànossy L. Cosmic Rays. Oxford, 1948.
18. *Goryachev B. I. et al.* // J. At. Nucl. 1973. V. 17. P. 463.
19. *Caldwell J. T. et al.* // Phys. Rev. C. 1984. V. 21. P. 1215;
Veyssiere A. et al. // Nucl. Phys. A. 1973. V. 199. P. 45;
Arrudantro J. D. T. et al. // Phys. Rev. C. 1976. V. 14. P. 1499.
20. *Goryachev B. I. at al.* // Pis'ma ZhETF. 1968. V. 7. P. 210;
Ishkhanov B. S. et al. // J. of Nucl. Phys. 1970. V. 12. P. 628;
Fuller E. G., Hayward E. // Nucl. Phys. 1962. V. 33. P. 431;
Veyssiere A. et al. // Nucl. Phys. A. 1970. V. 159.
21. *Bergere R., Beil H., Veyssiere A.* // Nucl. Phys. A. 1968. V. 121. P. 463;
Bramblett R. L. et al. // Phys. Rev. 1963. V. 120. P. 2723.
22. *Ericson M., Rosa-Clot M.* // Z. Phys. A. 1991. V. 324. P. 373;
Baumann B. et al. // Phys. Rev. C. 1988. V. 38. P. 1940;
Hayward E. // Phys. Rev. C. 1989. V. 40. P. 467.
23. *Leprêtere A. et al.* // Nucl. Phys. A. 1981. V. 367. P. 237.
24. *Leprêtere A., Bergêre R., Bourgeois P. et al.* // Nucl. Phys. A. 1987. V. 472. P. 533.
25. *Ryckbosch D., Carlos P., Leprêtere A.* // Z. für Fis. A. 1988. V. 329. P. 451.
26. *Veyssiere A. et al.* // Nucl. Phys. A. 1968. V. 121. P. 463;
Veyssiere A. et al. // Nucl. Phys. A. 1970. V. 159. P. 561;
Blatt J. M., Weisskopf V. F. Theoretical Nuclear Physics. New-York; London, 1952;
Berman B. L., Fultz S. C. // Rev. Mod. Phys. 1975. V. 47. P. 739;
Barret R. F. // Nucl. Phys. A. 1973. V. 210. P. 355.

27. *Frohner F. H.* // Nucl. Sci. Eng. 1988. V. 103. P. 251.
28. *McDaniels D. K.* // Nucl. Phys. A. 1982. V. 384. P. 88;
Darke D., Bergqwist M. I., McDaniels D. K. // Phys. Lett. B. 1971. V. 36. P. 557.
29. GELINA Neutron Time-of-Flight Facility. http://irmm.jre.ec.europa.eu ;
Flaska M. et al. // NIM. A. 2004. V. 531. P. 392.
30. *Klug J. et al.* // NIM. A. 2007. V. 577. P. 641;
Altstadt E. et al. // An. Nucl. Energy. 2007. V. 34. P. 36.
31. *Kim G. N. et al.* // NIM. A. 2002. V. 485. P. 458.
32. *Bockhoff K. H.* Properties of Neutron Sources // Proc. of Advisory Group Meeting on Properties of Neutron Sources. Leningrad, USSR, 9–13 June, 1986. IAEA-TECDOC-410, Vienna, 1987. P. 35–55.
33. *Harvey R. R. et al.* // Phys. Rev. B. 1964. V. 136. P. 126.

Received on December 14, 2010.

Корректор *Т. Е. Попеко*

Подписано в печать 21.02.2011.
Формат 60 × 90/16. Бумага офсетная. Печать офсетная.
Усл. печ. л. 1,43. Уч.-изд. л. 1,93. Тираж 290 экз. Заказ № 57280.

Издательский отдел Объединенного института ядерных исследований
141980, г. Дубна, Московская обл., ул. Жолио-Кюри, 6.
E-mail: publish@jinr.ru
www.jinr.ru/publish/